Journal of ELECTRONIC MATERIALS, Vol. 44, No. 6, 2015
DOI: 10.1007/s11664-015-3638-3

Thermoelectric Exhaust Heat Recovery with Heat Pipe-Based Thermal Control

F.P. BRITO,[1,3] JORGE MARTINS,[1] ESRA HANÇER,[2] NUNO ANTUNES,[1] and L.M. GONÇALVES[1]

1.—Universidade do Minho, Guimarães, Portugal. 2.—Erciyes University, Kayseri, Turkey. 3.—e-mail: francisco@dem.uminho.pt

Heat pipe (HP)-based heat exchangers can be used for very low resistance heat transfer between a hot and a cold source. Their operating temperature depends solely on the boiling point of their working fluid, so it is possible to control the heat transfer temperature if the pressure of the HP can be adjusted. This is the case of the variable conductance HPs (VCHP). This solution makes VCHPs ideal for the passive control of thermoelectric generator (TEG) temperature levels. The present work assesses, both theoretically and experimentally, the merit of the aforementioned approach. A thermal and electrical model of a TEG with VCHP assist is proposed. Experimental results obtained with a proof of concept prototype attached to a small single-cylinder engine are presented and used to validate the model. It was found that the HP heat exchanger indeed enables the TEG to operate at a constant, optimal temperature in a passive and safe way, and with a minimal overall thermal resistance, under part load, it effectively reduces the active module area without deprecating the temperature level of the active modules.

Key words: Thermoelectric generator, exhaust heat recovery, TEG modelling, heat pipes, thermal management, heat exchangers

List of symbols

Abbreviations

1D	One-dimensional
3D	Three-dimensional
EREV	Range extended electric vehicle
HEV	Hybrid electric vehicle
HP	Heat pipe
IC	Internal combustion
ORC	Organic rankine cycle
TE	Thermoelectric
TEG	Thermoelectric generator
VCHP	Variable conductance heat pipe

Variables

c_p	Specific heat at constant pressure (J kg^{-1} K^{-1})
g	Acceleration of gravity (m s^{-2})
h_c	Contact heat transfer coefficient (W m^{-2} K^{-1})
H_L	Enthalpy of vaporisation (J kg^{-1})
I	Electric current (A)
k	Thermal conductivity (W m^{-1} K^{-1})
k_l	Thermal conductivity of liquid (W m^{-1} K^{-1})
L_c	Active length of the condenser (m)
$\dot{m}$	Mass flow rate (kg s^{-1})
N_{pairs}	Number of (P–N) pairs in a thermoelectric module
n_{teg}	Number of thermoelectric modules
P_{max}	Electrical output power at matched load (W)
$\dot{Q}$	Thermal power (W)
$\dot{q}$	Thermal power generated per unit volume (W m^{-3})
R	Thermal resistance (K W^{-1})
$Ri_{total_{system_e}}$	Total electrical resistance of the module (Ω)
S	Shape factor (m^{-1})
T	Temperature (K)
T_s	Saturation temperature of the working fluid
T_{cond_w}	Temperature of the condenser wall

(Received July 20, 2014; accepted January 8, 2015; published online February 10, 2015)

V_o	Open circuit voltage (V)
α	Seebeck coefficient (V K^{-1})
η	Effectiveness of heat exchanger
μ_l	Dynamic viscosity of the liquid (Pa s)
ρ	Electrical resistivity (Ω m)
ρ_c	Contact resistivity (Ω m^2)
ρ_l	Density of the liquid (kg m^{-3})

Subscripts

BiTe	Thermoelectric material/legs
cold	Cold side of the thermoelectric generator
coolant	Liquid for cooling the cold face of TEG
downstream	Downstream of the module (in terms of heat flux direction)
e	Electric
evap	Evaporator (sector1)
exh	Exhaust gases
hot	Hot side of the thermoelectric generator
hot junction	Corresponding to the power leaving the hot junction
HP	Heat pipe
in	At the inlet
Joule total	Total Joule power generated within all the legs
l	Liquid
out	At the outlet
Peltier	By Peltier effect
Sector1	Evaporator region
Sector2	Condenser region (including coolant system)
TEG	Thermoelectric generator module
total	Corresponding to all legs, not just one leg
upstream	Upstream of the module (in terms of heat flux direction)

INTRODUCTION

Motivation

The automotive industry is facing ever more stringent goals in terms of energy efficiency and emissions (both of pollutants and greenhouse gases).[1] A substantial improvement in overall vehicle efficiency can be attained by increasing the internal combustion (IC) engine efficiency. This may be done through strategies such as overexpansion, as explored by the group,[2–4] but additional measures are required. Vehicle hybridization is one of them, as it enables the deployment of strategies such as regenerative braking energy, efficient urban electric-assisted driving and allows the use, to a higher degree, of the more efficient electric-driven components.[5,6]

However, the most abundant source of waste IC engine energy is the energy contained in exhaust gases, which is of the same order of magnitude as the mechanical energy provided to the driveshaft.[7,8] Also, from the second law of thermodynamics standpoint, it displays a good recovery potential due to its relatively high temperature. The gradual increase of vehicle electrification levels such as the one encountered in current hybrid electric vehicles (HEV) or range-extended electric vehicles (EREV) makes the conversion of some of the exhaust waste heat into electricity an attractive solution.[5] While the group has been exploring the concept of an efficiency-oriented range extender based on over-expansion,[9] the addition of exhaust-recovered electric energy would make all the sense for such applications. Moreover, IC engines working as generators have well-defined operating conditions, allowing for the optimization of the waste exhaust heat recovery system. Even conventional vehicles would gain with the harvesting of this energy by reducing the load of the alternator or even being able to eliminate its need altogether.[10,11]

Thermoelectric Generators

One of the ways for harvesting exhaust energy is by using thermoelectric (TE) modules based on the Seebeck effect. Although they still display efficiencies lower than thermodynamic cycle based systems such as organic rankine cycle (ORC) systems,[12] newly developed materials displaying better efficiencies are steadily appearing. This is the case for TE using nanostructured materials.[13] Unlike bulky ORC systems, thermoelectric generators (TEG) are intrinsically scalable and therefore suitable for low power ranges still not achieved by ORCs.[14] Furthermore, they are reliable as they possess no moving parts.

Some of the major challenges for the adoption of TEGs in automotive applications are related to their still low-power density and high cost, as well as their thermal management.[15]

There is ongoing research into materials which simultaneously display high TE conversion figure-of-merit[16] and do not use bulk rare earth materials. In this respect, some promising technologies for automotive applications include the use of magnesium silicides, zinc antimonide, skutterudite and half-heusler-based materials.[10,17] Real world exhaust heat recovery applications are being explored by several companies with these promising materials, but enhancements on their chemical (e.g. oxidation) and/or physical (e.g. sublimation) stability are still being overcome. In the meantime, the optimization of current commercially available module materials, such as those based on bismuth telluride, seems to be a more readily available solution. This could be done by finding ways of reducing the thickness of modules without damaging their output, as explored by the authors.[18] For this to happen, very low overall heat paths leading to the active TE junctions must exist.[19] Therefore, TEGs still need improve-

ments in terms of thermal management. On the one hand, modules are temperature-limited, but on the other hand their output increases as the temperature increases. It is therefore desirable that the temperature the modules will encounter should always be as high as they are able to safely withstand. Therefore, not only is there a need for a low overall heat exchanger resistance but also a suitable control of the operating temperature should be present. So there is clearly the need for a system with the aforementioned characteristics and possessing the capability of operating efficiently under variable thermal load.

Currently, the protection against module overheating during excess thermal load events involves the bypass of exhaust gases, which means wasting the most valuable driving cycle events in terms of exhaust energy. An alternative would be to convert the temperature of the heat reaching the TEGs to the optimal level, irrespective of engine load.[20,21]

Heat Pipes

The scope of the group's work is to overcome the aforementioned thermal management shortcomings using heat pipe (HP) heat exchangers, and specifically variable conductance heat pipes (VCHP).[22] HPs (see Fig. 1) are very simple heat transfer elements displaying a very high heat transfer rate due to their principle of operation based on phase change. They basically consist of a pipe containing a phase change fluid which boils as it absorbs heat from the heat source (in the present case, the exhaust gases). Vapour then rises and releases the heat through condensation to the heat sink (in the present case, the TE modules). The condensed fluid then falls back to the HP evaporator through gravity or through capillarity effect (e.g. wettability), as in the case of an HP with an inner wick (not used in the present case).[22]

Some specific advantages of using HP-based heat exchangers with TEGs rely on the fact that they are not in direct contact with the exhaust circuit. Therefore, their location is more flexible and, in the case of the VCHP, there is no need for waste gate/bypass valves, since excess exhaust temperature is passively downgraded. This occurs because the operating temperature is the fluid boiling temperature, which solely depends on its pressure. This pressure can be made fairly constant with the addition of a small expansion tank (see Fig. 2). This tank enables a near-constant pressure irrespective of load, because there is enough volume for the steam accommodation without incurring a significant pressure rise. The VCHP pressure may be pre-regulated in order to obtain the desired fluid boiling temperature. The variation of thermal load from the exhaust will be translated into a variable active length of the condenser (the length reached by the vapour) rather than into a variable operating temperature (the case of standard HPs). This results in no thermal dilution of the system, as only the necessary amount of modules will be active, working at the optimized temperature (e.g. a kind of cascading operation).

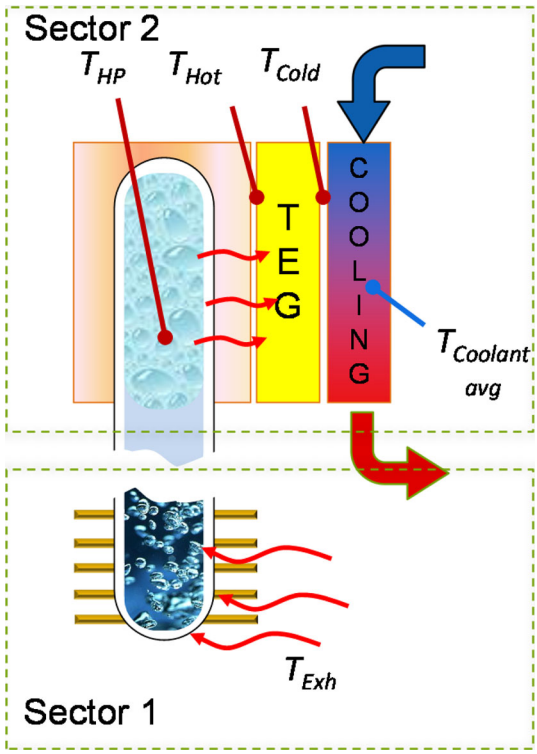

Fig. 1. Outline of the operation of a heat pipe heat exchanger.

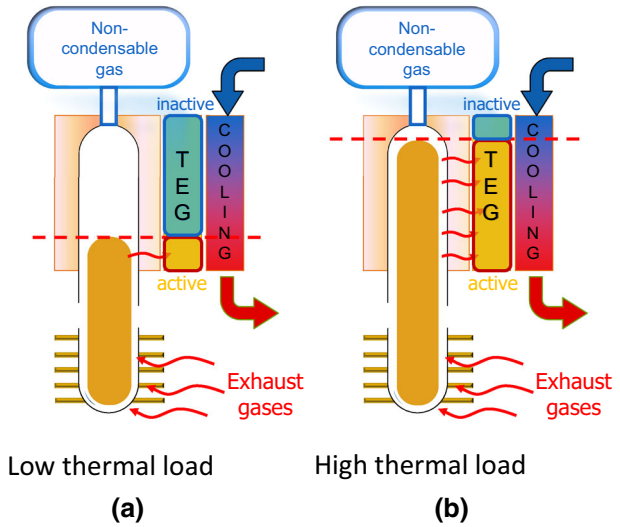

Fig. 2. Outline of the operation of a variable conductance heat pipe heat exchanger under (a) low thermal load and (b) high thermal load.

Proposed Approach

The present approach was originally proposed by the authors in some earlier publications. Several simplified proof of concept prototypes were tested using a propane blowtorch heat source,[21,23] along

with some simplified system modelling.[24] The influence of HP temperature on TEG output was assessed for a limited number of HP temperatures and with the generator attached to a small 10HP diesel engine, demonstrating the scalability of the system.[20] It was found that there is an optimal HP temperature which maximizes output, and expressions were derived to estimate the maximum output for given conditions and a given global heat exchanger effectiveness. The present work carries out a detailed modelling of the condenser part of a VCHP and of the thermoelectric modules, and also presents some experimental results performed for a broad set of conditions. Although the approach is one-dimensional (1D), it incorporates procedures which compensate for three-dimensional (3D) effects and takes into account all heat sources and sinks due to the diffuse Joule effect, contact resistance Joule effect and localized Peltier heat sources and sinks.

MODEL

Generator Modelling

Figure 1 shows an outline of the HP system. Since the HP temperature (T_{HP}), is constant, the evaporator (sector 1) and the condenser (sector 2) thermal powers ($\dot{Q}_{sector1}$ and $\dot{Q}_{sector2}$) may be calculated independently:

$$\dot{Q}_{sector1} = \frac{\bar{T}_{exh\_in} - T_{HP}}{R_{sector1}}; \quad \dot{Q}_{sector2} = \frac{T_{HP} - \bar{T}_{coolant}}{R_{sector2}}, \tag{1}$$

where T_{exh_in} is the inlet exhaust gases temperature, $T_{coolant}$ is the temperature of the coolant fluid of the TEG and $R_{sector1}$ and $R_{sector2}$ are the total thermal resistances of the evaporator and condenser regions. The actual thermal power crossing the generator will be the lower of the two. This is so because the condenser will not be able to absorb excess boiling power, while some of the condenser power capacity will not be used if insufficient evaporator power is present. So, the effective power curve of the apparatus will be the lower envelope of the evaporator and condenser power curves:

$$\dot{Q}_{total} = \min\left(\dot{Q}_{sector1}; \dot{Q}_{sector2}\right). \tag{2}$$

This allows the definition of the load of the condenser ($Load_{cond}$) as follows:

$$Load_{cond} = \frac{\dot{Q}_{total}}{\dot{Q}_{sector2}} \tag{3}$$

This will be the fraction of the generator length which will be active, as depicted in Fig. 2. Therefore, all output variables (e.g. thermal power, voltage, electric power) will correspond to a fraction $Load_{cond}$ of the full load values. If, for a given set of conditions, the load is always 100%, this means that the generator's condenser is undersized for the application and that more modules and a bigger condenser could be used to harvest more exhaust power. If the condenser load is much lower than 100%, it means that the amount of modules used and the size of the condenser are excessive for the application or at least that the exhaust power absorbed by the heat pipes is too low. This implies that only a fraction of the total number of TEGs will be active.

Sector 1 (Exhaust–HP Interior)

Exhaust heat can only be absorbed as long as its temperature (T_{exh_in}) is higher than T_{HP} (see Fig. 1). Therefore, the higher is T_{HP}, the lower will be the available (absorbable) exhaust thermal power $\left(\dot{Q}_{available}\right)$ for a given mass flow of gases ($\dot{m}_{exh}$) at a given inlet temperature (T_{exh_in}):

$$\dot{Q}_{available} = \dot{m}_{exh} \cdot c_{p\_exh} \cdot (T_{exh\_in} - T_{HP}) \tag{4}$$

with $c_{p\_exh\_in}$ being the specific heat of the inlet gases.

The effectiveness of the evaporator is therefore defined as follows:

$$\eta_{evap} = \frac{\dot{Q}_{sector1}}{\dot{Q}_{available}} \tag{5}$$

Some heat transfer modelling has been performed to estimate the global thermal resistance of Sector 1. The convection at the finned heat exchanger was modelled with the Zukauskas[25] expression for a flow over a staggered tube bank and the finned surface efficiency was also estimated.[26] Then, the Rohsenow expression for nucleate boiling was used.[22] Unfortunately, the results were not satisfactory. Surprisingly, though, when considering a constant evaporator effectiveness (based on available power) of 40%, a quite good correlation with the experimental results was obtained. This low value might be related to the highly oxidized and fouled state of the heat exchanger. Therefore, the evaporator modelling at this stage consisted solely of imposing a constant heat exchanger effectiveness of 40% based on the available power:

$$\dot{Q}_{sector1} = \eta_{evap} \cdot \dot{Q}_{available}. \tag{6}$$

Sector 2 (HP Interior–TEGs–Cooling Ducts)

The Nusselt theory for film condensation over a condenser of active length L_c was implemented[22] to calculate the average heat transfer coefficient, h_{cond}:

$$h_{cond} = 0.943\left[\frac{H_L \rho_l^2 g k_l^3}{L_c \mu_l (T_s - T_{cond\_w})}\right]^{0.25} \tag{7}$$

where H_L is the enthalpy of vaporization of the liquid, ρ_l is the density of the liquid, g is the acceleration of gravity, k_l is the thermal conductivity of the liquid, μ_l is

the dynamic viscosity of the liquid, T_s is the saturation temperature of the fluid (considered to be T_{HP}) and T_{cond_w} is the temperature of the condenser wall.

Concerning the estimation of the thermal resistances corresponding to the heat transfer by conduction through solids, the 1D approach poses a difficulty, since there is a 3D heat path. Fortunately, it is possible to use the conduction shape factor concept (S), which allows the calculating of the 1D thermal resistance equivalent of a 3D shape in situations where a non-uniform section area and thickness exist. In practical terms, S stands out as an equivalent "section area to thickness ratio" in the conduction thermal resistance expression[26]:

$$R_{\text{Cond}} = \frac{1}{Sk}; \quad S = \left(A/t\right)_{\text{eq}} \tag{8}$$

Expressions to calculate shape factors are available for a limited range of reference geometries. The solution used to derive the shape factor for the condenser blocks, cooling ducts and some TEG sections was to simulate those geometries in a solver (e.g. ANSYS CFX) for a given temperature difference (ΔT) across their thermal inlet and outlet faces, then extract the thermal power, and finally deduce S from the following formula:

$$\dot{Q} = \frac{\Delta T}{R_{\text{Cond}}} = Sk\Delta T \tag{9}$$

The value calculated for S will be universal, that is, independent of ΔT because it is a geometric parameter.

The thermal contact resistances are calculated from the contact heat transfer coefficient (h_c) and the corresponding section area (A):

$$R_c = \frac{1}{h_c A}. \tag{10}$$

Some values for the contact heat transfer coefficients for specific pairs of contact, for various contact pressures and for various interstitial media (e.g. vacuum, air, thermal grease) are available in the literature.[27–30] Thermal grease was used at the module interfaces with the condenser walls (hot face) and the cooling plate walls (cold face), so a value h_c = 19 kW m^{-2} K^{-1} (silicone oil thermal grease[27]) has been considered. Unfortunately, no information has been found in the literature regarding typical thermoelectric generator internal interfaces (e.g. aluminium oxide/copper conductor/$BiTe_3$ interfaces). These values are likely to vary significantly depending on the manufacturer, and on the materials and manufacturing processes used. One source displays values for bonded surfaces used in power electronics (silicon chip/aluminium with 0.02-mm epoxy[28]). These display average contact heat transfer coefficients close to the ones used for interfaces with silicone oil thermal grease. Therefore, and although this issue still deserves further investigation, the present work has opted to use a uniform value for all the interfaces (h_c = 19 kW m^{-2} K^{-1}).

Sector 2—Detailed TEG Modelling

Concerning the modelling of the TE modules, analytical 1D expressions for the estimation of thermal power and temperature have been derived. One challenge of the conventional 1D heat transfer models is the existence of diffuse heat sources due to the Joule effect within the materials with current flow. These diffuse heat sources cannot be correctly simulated using the conventional equivalent electric circuit analogy. However, there is an analytical solution for the temperature field within a medium with a diffuse and uniform heat source ($\dot{q}$)[26]:

$$T(x) = -\dot{q}/2k x^2 + C_1 x + C_2; \quad \dot{q} = -\frac{\dot{Q}_{\text{Jouletotal}}}{A_{\text{BiTe\_total}} \cdot l_{\text{BiTe}}} \tag{11}$$

where $\dot{Q}_{\text{Jouletotal}}$ is the total Joule thermal power generated within the legs of all modules, $A_{\text{BiTe\_total}}$ is the total section area of all legs, l_{BiTe} is the thickness of a TEG leg, and C_1 and C_2 are the constants of the equation, to be determined, and with $\dot{q}$ having the units of thermal power generated per unit volume. In the case of a TE element leg such as the one outlined in Fig. 3, the following conditions apply:

$$T(0) = T_{\text{TEG}_{\text{hot}}} \rightarrow C_2 = T_{\text{TEG}_{\text{hot}}} \tag{12}$$

$$\begin{aligned} -k_{\text{BiTe}} A_{\text{BiTe\_total}} \frac{\mathrm{d}T(0)}{\mathrm{d}x} &= \dot{Q}_{\text{hot junction}} \\ \rightarrow C_1 &= -\frac{\dot{Q}_{\text{hot junction}}}{k_{\text{BiTe}} A_{\text{BiTe\_total}}} \end{aligned} \tag{13}$$

With $\dot{Q}_{\text{hot junction}}$ being the total thermal power (all modules) leaving the hot face of the TE material (as defined in Fig. 3), $T_{\text{TEG}_{\text{hot}}}$ the temperature at the hot face of the TE element and k_{BiTe} the average thermal conductivity of the TE legs. The temperature distribution along the TE element may be calculated anywhere along the TE material thickness applying these conditions to (11). Of special interest is the temperature difference across the active TE leg junctions because it is the one responsible for the Seebeck voltage:

$$\begin{aligned} T_{\text{TEG}_{\text{hot}}} - T_{\text{TEG}_{\text{cool}}} = &\left(\dot{Q}_{\text{hot junction}} + \frac{\dot{Q}_{\text{Jouletotal}}}{2}\right) \\ &\times \frac{l_{\text{BiTe}}}{k_{\text{BiTe}} A_{\text{BiTe\_total}}} \end{aligned} \tag{14}$$

where $T_{\text{TEG}_{\text{cool}}}$ is the temperature of the cold face of the TE element. Some of the module's layers will display strong 3D heat flux, something which is not suitably treated with a 1D approach. For instance, the heat entering the whole module through the alumina will be channelled only through the metal

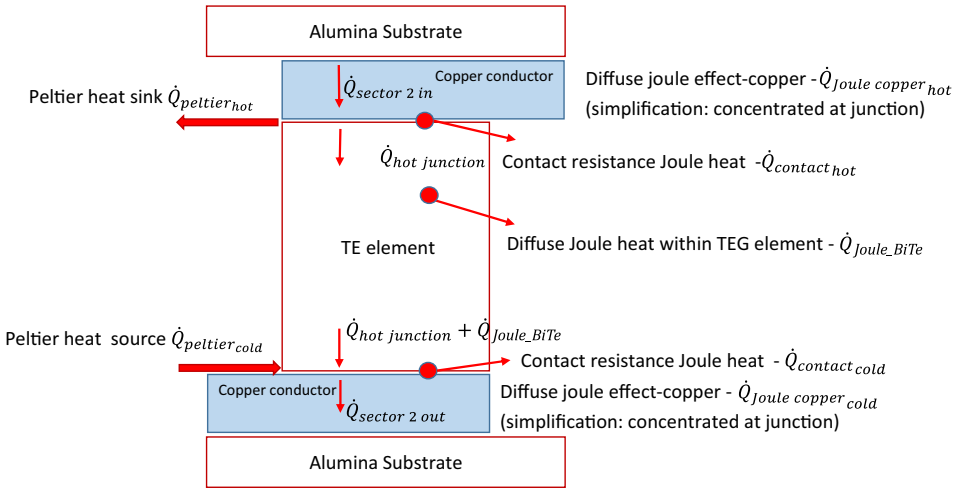

Fig. 3. Outline of the heat fluxes, including heat sources and sinks within a thermoelectric element.

conductors interface, that is, the heat inlet area will be higher than the outlet area. The same 3D heat flux will exist across the metal conductors: the heat reaching the metal conductors coming from the alumina substrate will be channelled into the TE element leg interface, which is smaller. However, it is possible to deduce conductive shape factors according to Eqs. 8 and 9 to compensate for these 3D effects, keeping a 1D heat transfer approach. The shape factors for alumina and metal conductors were calculated with a commercial solver (ANSYS CFX) and using Eq. 9. Since S is a geometric parameter, it will not depend on thermal inputs, only on the corresponding geometry.

Once the circuit is closed with a resistive load, the Seebeck voltage will induce a current. The Joule effect will be present within the TE elements $\left(\dot{Q}_{\text{Joule\_BiTe}}\right)$ and the copper conductors $\left(\dot{Q}_{\text{Joule\_copper}}\right)$. Localized heat sinks and sources due to the Peltier effect ($\dot{Q}_{\text{Peltier}_{\text{hot}}}$ and $\dot{Q}_{\text{Peltier}_{\text{cold}}}$) will appear at the hot and cold junctions of the TE materials, respectively.[31] Also, localized heat sources due to electric contact resistance Joule effect $\left(\dot{Q}_{\text{Joule}_{\text{contact}}}\right)$ will appear at those junctions (see Fig. 3):

$$\dot{Q}_{\text{Peltier}_{\text{hot}}} = -\alpha_{\text{BiTe}_{\text{pair}}} * T_{\text{TEGhot}} * I * N_{\text{pairs}} * n_{\text{TEG}} \tag{15}$$

$$\dot{Q}_{\text{Peltier}_{\text{cold}}} = \alpha_{\text{BiTe}_{\text{pair}}} * T_{\text{TEGcold}} * I * N_{\text{pairs}} * n_{\text{TEG}} \tag{16}$$

$$\dot{Q}_{\text{Joule}_{\text{contact}}} = {}^{\rho_C}/_{A_{\text{BiTe\_total}}} * I^2 \tag{17}$$

$$\dot{Q}_{\text{Joule\_BiTe}} = {}^{\rho.l}/_{A_{\text{BiTe\_total}}} * I^2, \tag{18}$$

$\alpha_{\text{BiTe}_{\text{pair}}}$ is the Seebek coefficient of the P–N junction ($\alpha_P - \alpha_N$), I the Seebeck-induced current, N_{pairs} the number of thermoelectric P–N pairs per module, n_{TEG} the number of thermoelectric modules, ρ_C the electrical contact resistivity, ρ the electrical resistivity of TE element material, l the TE element length and $A_{\text{BiTe\_total}}$ the total contact area (between TE elements and metal). Due to these heat sources/sinks, the thermal power will vary slightly along the heat path. According to the Fourier law of cooling,[26] the heat generated will always flow in the opposite direction to the thermal gradient. Therefore, unless these heat sources are so strong that they create local temperature maximums/minimums (in which case, heat flux would occur in both directions), the localized heat generated will flow in one direction only, the opposite direction to the thermal gradient.

In the absence of heat sources/sinks, the thermal power between two generic nodes 1 and 2, $\dot{Q}_{1:2}$, will be a function of the corresponding thermal resistance ($R_{1:2}$) and of the temperature differential ($T_1 - T_2$):

$$\dot{Q}_{1:2} = \frac{T_1 - T_2}{R_{1:2}} \tag{19}$$

It is possible to use this equation along all the nodes of a 1D heat path where only the temperature of the extreme nodes is known, and express the temperature of a node as a function of the adjacent one:

$$\dot{Q}_{23} = \frac{T_2 - T_3}{R_{23}} \Rightarrow T_2 = T_3 + R_{23}\dot{Q}_{23};$$
$$T_3 = T_4 + R_{34}\dot{Q}_{34}; \quad \ldots T_{n-1} = T_n + R_{n-1n}\dot{Q}_{n-1n}. \tag{20}$$

The thermal powers crossing each node will not always be constant due to the heat sources and sinks present (Fig. 3), which are obtained from Eqs. 15–18. The current will be a result from the Seebeck effect calculations, but it may initially be assumed to be zero and then is corrected after each iteration.

By carrying out a backward substitution of these equations into one another and finally into Eq. 19, it is possible to eliminate temperature unknowns and obtain an expression for the thermal power as a function of known parameters, such as the temperatures of the nodes located at the extremities of the heat path. In the present case, the temperatures at the extremities of the heat path are the heat pipe temperature (T_{HP}), which is known, and the average coolant temperature ($\bar{T}_{coolant}$) which is obtained from $T_{coolant\_in}$, and from the power transmitted to the coolant ($\dot{Q}_{coolant}$):

$$\dot{Q}_{coolant} = \dot{m}_{coolant} c_{p\_coolant} (T_{coolant\_out} - T_{coolant\_in}), \tag{21}$$

where $\dot{m}_{coolant}$ and $c_{p\_coolant}$ are the mass flow rate and specific heat of the coolant. Of course, $\dot{Q}_{coolant}$ is unknown. Nonetheless, it may be initially assumed as being zero and then corrected iteratively once the thermal power transmitted to the water has been determined in each iteration.

Using the aforementioned substitution method, the following expression for the estimation of the total thermal power reaching the module from the condenser has been derived (see Fig. 3):

$$\dot{Q}_{sector2\,in} = \frac{\left(T_{HP} - \bar{T}_{coolant} - \left(\left(\dot{Q}_1 + \left(\frac{\dot{Q}_{Joule\_BiTe}}{2}\right)\right) * R_{BiTe}\right) - \dot{Q}_2 * (R_2 + R_{downstream})\right)}{R_1 + R_2 + R_{downstream} + R_{BiTe}} \tag{22}$$

with R_{BiTe} being the thermal resistance of the TE elements and $R_{downstream}$ being the thermal resistances downstream of the module. Also, $\dot{Q}_1$, $\dot{Q}_2$, R_1 and R_2 are defined as follows:

$$\begin{aligned} \dot{Q}_1 &= -\dot{Q}_{Peltier_{hot}} + \dot{Q}_{contact_{hot}} + \dot{Q}_{Joule\,copper_{hot}} \\ \dot{Q}_2 &= \dot{Q}_{Joule\,copper_{tot}} + \dot{Q}_{Peltier_{tot}} + \dot{Q}_{contact_{tot}} + \dot{Q}_{Joule\_BiTe} \end{aligned} \tag{23}$$

$$\begin{aligned} R_1 &= R_{copper_{hot}} + R_{ceramichot} + R_{upstream} \\ &\quad + R_{contact_{ceramic copper_{hot}}} + R_{contact_{copper BiTe_{hot}}} \\ R_2 &= R_{copper_{cold}} + R_{ceramiccold} + R_{contact_{ceramic copper_{cold}}} \\ &\quad + R_{contact_{copper BiTe_{cold}}} \end{aligned} \tag{24}$$

The subscripts hot and cold correspond to the hot or cold sides of the TEG, the ceramic and copper subscripts correspond to the alumina substrate and the metal conductors, respectively, while $R_{upstream}$ and $R_{downstream}$ include all the thermal resistances located upstream and downstream of the module, respectively. The upstream resistances include the condensation resistance (calculated through Eq. 7), the conduction resistance (Eq. 8) and the contact resistance (Eq. 10) between modules and condenser blocks (which had thermal grease in the experimental apparatus). Regarding the downstream parcel, there will also be the conduction and contact resistances, but the main contribution will be the convection resistance, which has been considered to be that of a developing flow inside a cooling duct (Sieder and Tate)[26]:

$$Nu = 1.86 \left(\frac{RePrD_h}{L}\right)^{1/3} \left(\frac{\mu_b}{\mu_s}\right)^{0.14}, \tag{25}$$

with Re, Pr and D_h being the Reynolds number, Prandtl number and the hydraulic diameter, respectively. L is the characteristic duct length. This characteristic length will not necessarily be the total length of the heat sink duct, which in the present case has a zig-zag profile, but the length which is representative of the phenomenon of flow developing inside a duct. Flow under development (flow within the so-called entry region) has a higher mixing degree than fully developed flow, in which the velocity profile has already stabilized. After flow obstacles or steep duct bends, flow development is re-initiated, and therefore the characteristic length to be used in Eq. 25 will be the length of one of the straight portions of the zig-zag heat sink ducts.

Having calculated $\dot{Q}_{sector2}$ it will then be possible to calculate the temperatures at each interface, starting from one of the known temperatures (e.g. T_{HP} or $\bar{T}_{coolant}$) and using Eq. 20. Of course, this will be an iterative process since, for instance, it will only be possible to estimate Peltier and Joule powers once the Seebeck effect has been calculated, and Seebeck voltage and current calculations require the temperature field to be calculated, and so on. Also, the temperature-dependent physical properties need to be updated at the end of each iteration. The expressions for the open circuit voltage (V_o) and for the maximum power (P_{max}) at matched load (load resistance equalling the internal resistance) are as follows:

$$V_o = n_{TEG} * N_{pairs} * \alpha_{BiTe_{pair}} * (T_{TEG\_hot} - T_{TEG\_cold}) \tag{26}$$

$$P_{max} = \frac{V_o^2}{4R_{i_{total_{system_e}}}} \tag{27}$$

$\alpha_{BiTe_{pair}}$ is the Seebeck coefficient of the P–N thermoelectric junction ($\alpha_P - \alpha_N$), and R_i is the total electric

resistance (copper, contacts and thermoelectric element) of the system, often called the internal resistance of the system. The TEG_hot and TEG_cold subscripts correspond to the TE/copper junction temperatures at the hot side and the cold side, respectively.

Experimental Apparatus (Proof of Concept)

To enable the assessment of the merit of VCHP heat exchangers for the exhaust heat recovery from an IC Engine, a proof of concept was developed and built. This proof of concept prototype has already been described in detail in Ref. 20.

As previously explained, the TEG modules used in the present work cannot withstand temperatures above 250°C, but the exhaust of IC Engines might exceed 900°C, so the concept of temperature control by using pressure controlled HPs as heat transfer media was used. The temperature at which the heat transfer would occur was controlled by the manipulation of the HP pressure.

The present work uses the exhaust gases of a small diesel engine (Fig. 4) as the heat source, allowing a proof-of-concept testing and an illustration of the concept scalability. The heating power of the exhaust gases was within the range of the power that could be handled by the apparatus, but unfortunately the somewhat poor condition of the finned heat exchanger did not allow the exploration of the full potential of the thermal device.

The experimental apparatus is comprised of the following elements:

- Small internal combustion engine (Fig. 4), Yanmar L100N Diesel DI, with a shaft maximum power of 10 hp @ 3600 rpm and with a maximum exhaust flow rate of 0.02 kg s^{-1} @ ~350°C;
- Heat transfer device consisting of various heat pipes with the evaporator section being in contact with the hot exhaust gases (with fins) and the condenser section consisting of drilled flat copper blocks (Figs. 5 and 7);
- 12 TEG modules (ETDYN GM-250-49-45-25) attached to the three flat copper blocks of the HP (see Fig. 6);
- Water cooled heat sinks, attached to the cold face of the TEG modules, made from solid copper blocks with drilled channels, forming an internal zig-zag shape with a flow rate around 0.03 kg s^{-1} (Fig. 6).

The hot exhaust gases coming from the IC engine transfer their enthalpy to the finned copper tubes (Fig. 7), boiling the water contained within them (see Fig. 1). The generated steam travels upwards within the copper tubes and into the drilled holes of the condenser copper blocks, where it condenses. The heat from the phase change of the water travels across the TEG modules and is released to a flow of water that runs inside the heat sinks attached to the cold side of the TEG modules. Therefore, the heat path can be divided into the following sections (Fig. 5):

(a) exhaust gases from the IC engine to finned evaporator;
(b) from the fins and copper tube walls (8 mm outer diameter) to the boiling water as latent heat;

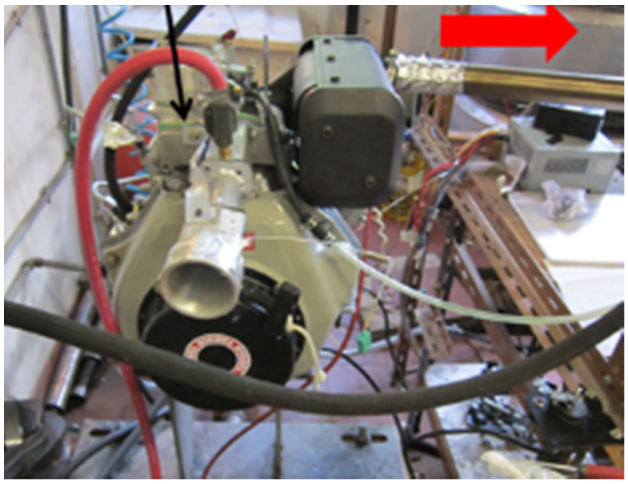

Fig. 4. Engine used (10 hp Yanmar L100N Diesel DI).

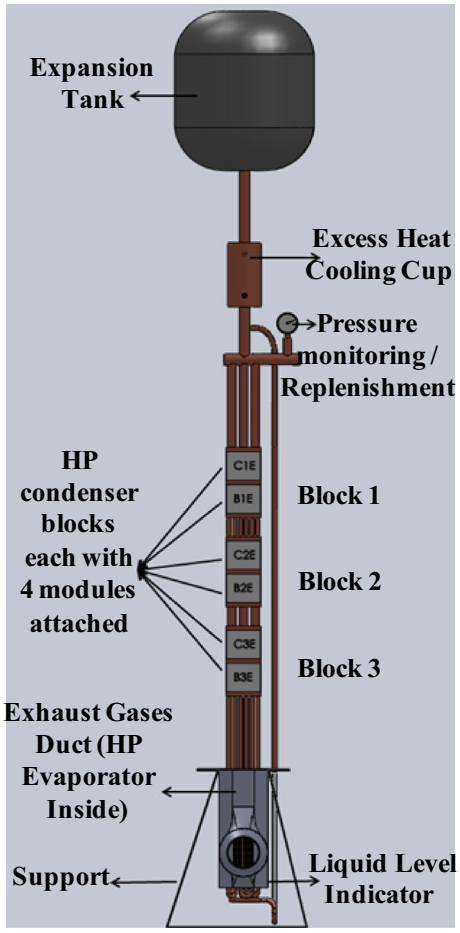

Fig. 5. Outline of the proof-of-concept heat pipe-based thermoelectric generator.

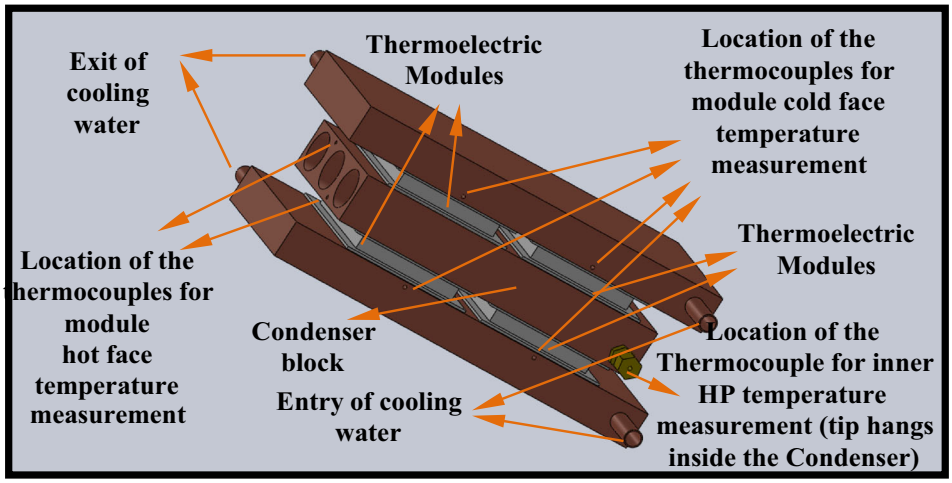

Fig. 6. One of the three HP condenser blocks each one attached with modules on both sides and external cooling ducts.

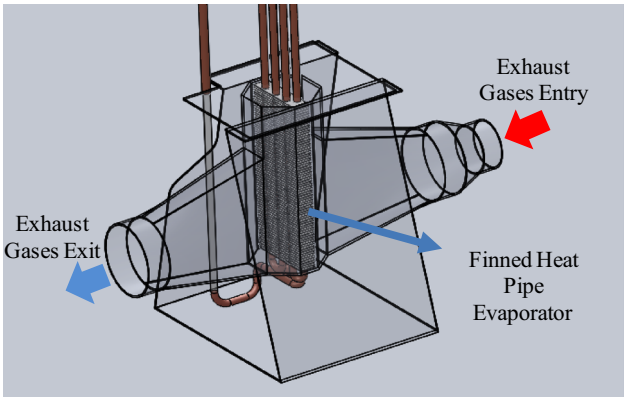

Fig. 7. Drawing of the exhaust gases duct with the finned HP Evaporator inside (6 pipes with 8 mm outer diameter).

(c) heat transport, through the vapour motion, from the evaporator to the condenser region;
(d) from the condensing water to the wall of the copper blocks;
(e) from the cooper blocks through the TEG modules to the heat sink material;
(f) finally the heat is withdrawn from the walls by the coolant flow.

The referred Sector 1 includes (a)–(c), whereas Sector 2 comprises (c)–(f). Several HP temperatures between 103°C and 188°C were tested, using water as phase change fluid.

Regarding temperature measurements, type K thermocouples were attached to a high-resolution 24-bit National Instruments data acquisition system NI 4350 with ±0.42-K thermocouple measurement accuracy. This accuracy affects the estimation of the thermal power, which is computed based on the temperature rise of the coolant flow. Thus, for the typical coolant flow rate used (80 L h^{-1}), a maximum error of ±37 W would be obtained in the thermal power estimation. The accuracy of the flow rate measurements will also affect the accuracy of the thermal power estimation. Although the flow rate was found to have little fluctuation over time (<±1%), it was recorded several times and averaged. This was done by measuring the time necessary to fill a 1-L graduated cup. A measurement accuracy of ±10 mL (corresponding to ±1% measurement accuracy) plus the effect of the flow rate fluctuation will roughly correspond to ±2% global accuracy of the flow rate estimation.

System voltages (both open and closed circuit) were measured by several National Instruments NI USB 6008 cards with 12-bit resolution and ±14.7-mV accuracy at room temperature. This represents a relative accuracy between ±0.7% and ±1.1% over the range of variation of the average open circuit voltage per module, under steady state conditions. Since the matched power output is a function of V_o^2, the effect of the latter parameter on the accuracy of the electric power will be between ±1.4% and ±2.2%. The load resistances used were Caddock MP930 Series TO-220 Radial Power Film Resistor with 0.5 Ω ± 1% each. Since the electric power is inversely proportional to the load, the variability of the load resistance will affect ±1% the estimation of the electric power. Therefore, the estimated value of the matched electric power will display a combined accuracy between 2.4% and 3.2% as a consequence of the accuracies of the open circuit voltage and the load resistance. The calculated accuracies seem to be sufficient for the purpose of the present work.

RESULTS AND DISCUSSION

Figure 8 shows the evolution of the inlet and outlet exhaust temperatures, the HP temperature and the average coolant temperature (water) along time for a sample HP pressure/temperature of 7.8 bar/168°C. On the one hand, it can be seen that the HP temperature stabilizes quickly at 168°C,

which is the boiling temperature corresponding to the pre-regulated pressure (7.8 bar). On the other hand, it can be seen that the heat exchanger effectiveness is not high, since there is still a lot of available ΔT between the outlet exhaust temperature and the HP temperature (the temperature the gases would achieve for 100% heat exchanger effectiveness).

Some more temperature plots of the same test are presented in Fig. 9. The hot and cold face temperatures of the TEGs are shown against the HP temperature. Low thermal resistances at the hot side of the TEG can be observed. For instance, the hot face temperature of condenser block 3 (the condenser block located lowest along the HP, as seen in Fig. 9b) is nearly equal to the HP temperature. So this block is working at full load (the vapour fully reaches it). While there are no temperature data for the intermediate condenser block 2, the temperature data for condenser block 1 (the highest located one) indicates that the vapour is reaching it only partially, so the generator is working at part load. This means that the evaporator is not producing enough vapour for the capacity of the condenser. The main reason for this is that there is not a lot of available exhaust power (the engine is rather small). Moreover, the effectiveness of the heat exchanger is low (only around 40% of the available exhaust heat is being absorbed). It is likely that this low effectiveness is mainly attributed to the convection-related thermal resistance rather than to the heat pipe boiling resistance, which is, typically, very low.

Figure 10 displays the thermal power that reaches the cooling water coming from each of the three condenser blocks. It has been computed by accounting for the temperature rise experienced by the coolant according to Eq. 21. The cascading operation of the system can be observed as the vapour reaches higher and higher up the various condenser blocks over time. Again, it can be observed that the upper condenser block never gets to operate at full load because there is not enough vapour

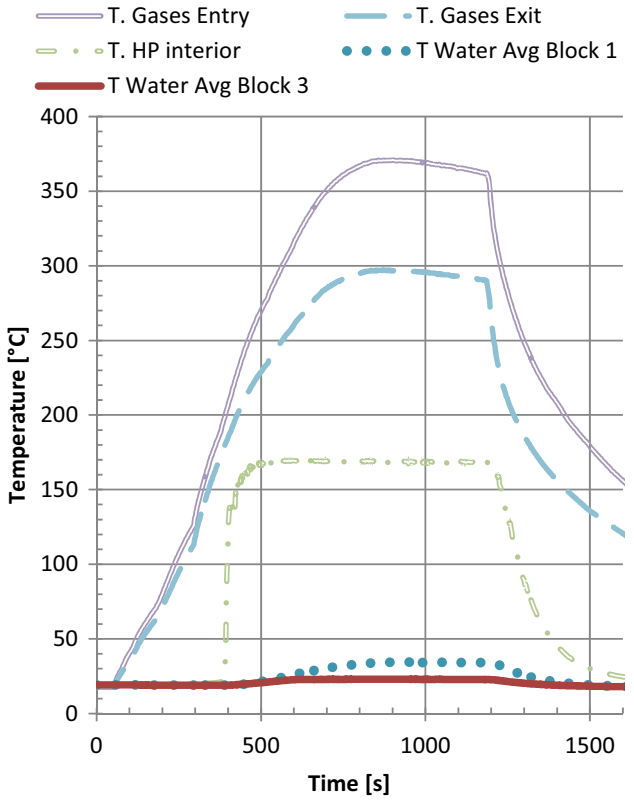

Fig. 8. Temperature results for an HP pressure/temperature of 7.8 bar/168°C.

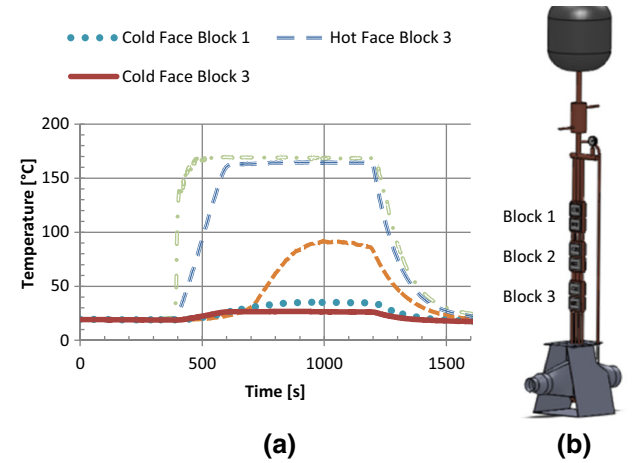

Fig. 9. (a) Temperature results for an HP pressure/temperature of 7.8 bar/168°C; (b) drawing of the prototype.

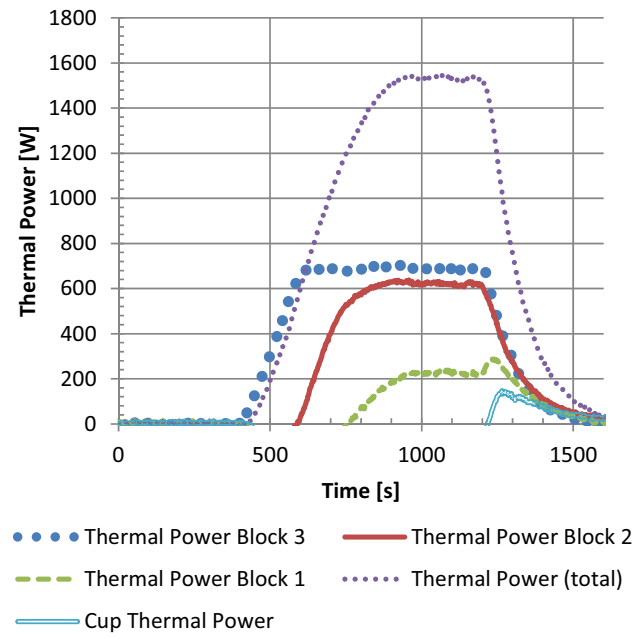

Fig. 10. Thermal power results for an HP pressure/temperature of 7.8 bar/168°C.

production (condenser capacity is higher than evaporator power).

The electric power of each block is represented in Fig. 11. This is the matched-load electric power of the generator. These values were obtained by measuring the open circuit voltage for half of the modules and measuring the closed circuit voltage for the other half of the modules using a load with a resistance similar to the internal resistance of the modules. These two values allowed the calculating of the internal resistance of the modules and to estimate the maximum output of the modules through Eq. 27. The same cascading operation can be observed in power output, as each block starts operating once the previous one has reached its full load.

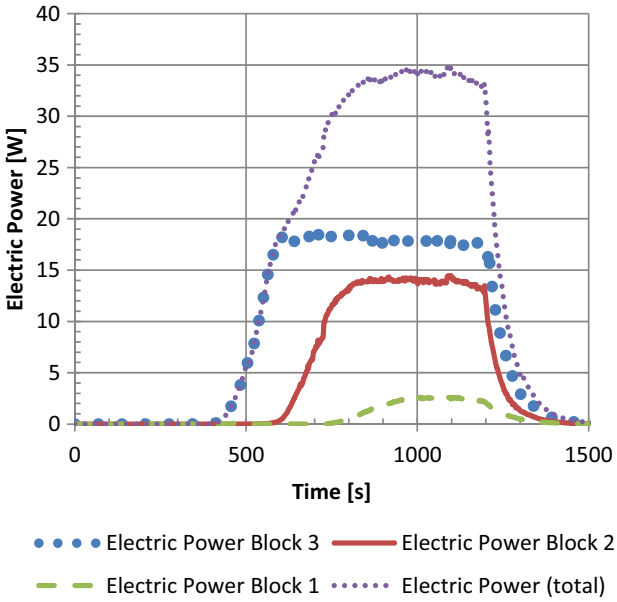

Fig. 11. Electric power for an HP pressure/temperature of 7.8 bar/168°C.

The first comparisons between predictions and experiments can be observed in Fig. 12, which represents the temperature profile (calculated and experimental) along the various material layers of Sector 2 (HP–TEG–Cooling system) for an HP pressure/temperature of 1.1 bar/103°C. The comparison can only be made at four different locations, and where temperatures have been recorded. In these locations the differences between theory and experiment are small. The white areas represent the several interfaces with their corresponding temperature fall due to thermal contact resistance. This figure is helpful to understand where the total available ΔT $\left(T_{\mathrm{hp}} - \bar{T}_{\mathrm{coolant}}\right)$ is being deprecated down to the useful ΔT, the one occurring between the hot and cold junctions of the active TE materials $\left(T_{\mathrm{TEG_{hot}}} - T_{\mathrm{TEG_{cool}}}\right)$, represented by the BiTe area in Fig. 12. It can be seen that the thermal resistance of the HP is very small, smaller than the thermal contact resistances of the interfaces. The importance of these phenomena for the output of TEGs is being investigated by the authors in a different article submission. These phenomena are especially relevant if the objective is to minimize TEG thickness to cut material costs.

Figures 13, 14 and 15 display the global, steady state predictions and experimental measurements for thermal power (Fig. 13), open circuit voltage (Fig. 14) and matched electric power (Fig. 15), respectively, for the whole HP pressure/temperature range tested (100–190°C).

The results for the thermal power reaching the coolant system can be observed in Fig. 13. Concerning the experimental results for each block, it can be observed that for low HP temperatures the power is low but all the blocks are fully operating, with similar thermal output. Thermal power increases as HP temperature increases, up to 160°C.

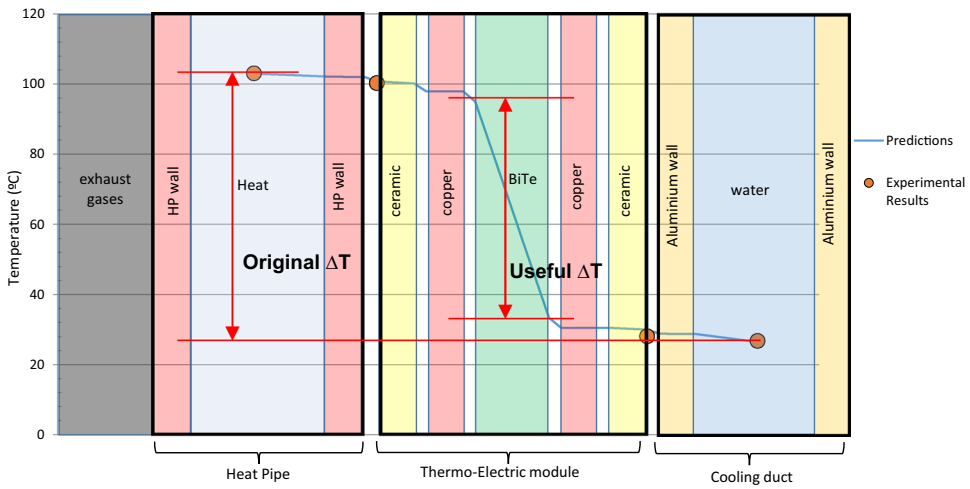

Fig. 12. Theoretical versus experimental temperature profile along Sector 2 (Condenser–TEG–water cooling ducts) HP pressure/temperature of 1.1 bar/103°C (white space represents temperature fade across interfaces due to thermal contact resistance.

As HP temperature increases, it can be observed that the power starts to drop at the upper condenser block (Block 1), then in the middle block (Block 2). As a consequence, the total thermal power output ($\dot{Q}_{coolant}$) decreases for HP temperatures above 160°C. The reason for this trend may be better understood by looking at the simulation results, which distinguish between evaporator power ($\dot{Q}_{sector1}$), and maximum condenser power (or condenser power capacity, $\dot{Q}_{sector2}$). According to Eq. 2, the effective thermal power crossing the generator will be the lower envelope of both these predicted curves, presented in Fig. 13, both for sector 1 (evaporator) and sector 2 (condenser). At low HP temperatures, and according to Eq. 6, the evaporator power is high because the available power, calculated through Eq. 4, is also high, due to the high temperature difference between the exhaust gases and the HP. On the contrary, under low HP temperatures, the condenser power capacity will be low: according to Eq. 1, and a low ΔT between HP and coolant will mean low power, for a given thermal resistance. Therefore, there will be excess boiling power not absorbed by the condenser blocks. This excess will only be absorbed by the auxiliary cooling cup (a concentric tube heat exchanger) located above the condenser blocks, as seen in Fig. 5. Therefore, at low HP temperatures, the condenser power capacity will be the lower of the two, being the limiting factor for the total thermal power.

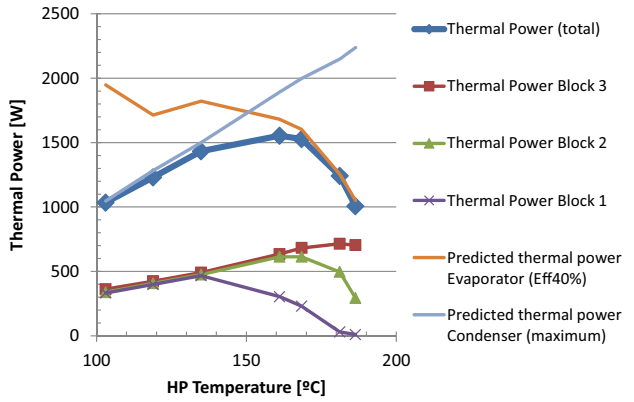

Fig. 13. Theoretical versus experimental steady state thermal power results for the whole HP pressure/temperature range tested.

At high HP temperatures, the opposite occurs, with the condenser power capacity being high and the evaporator power being low. So, at high temperatures, the condenser load, according to Eq. 3, will not be 100%, and therefore the thermal power, voltage and electric power will only be a fraction of the condenser power capacity. Therefore, the predicted evaporator–condenser total thermal power envelope is well in line with the measurements, and inclusively helps to better understand them.

The optimal HP temperature is found to be somewhere around 150°C. Below 150°C, more modules are active (higher available energy) but with less output capacity (low ΔT, Seebeck voltage). Above 150°C, the active modules have higher output capacity (high ΔT, high Seebeck voltage) but less thermal energy is available, so only a few of them will be operating. Of course, if higher thermal powers or evaporator efficiencies were available, then the evaporator power would not fall so steeply and therefore the optimum HP temperature would be higher.

The open circuit voltage and electric power plots, represented in Figs. 14 and 15, reflect what has been said concerning thermal power. These figures present both experiments and predictions. The predictions are within a small error range, with the differences in electric power being mainly attributed to the uncertainties in the internal resistance calculation from the open and closed circuit voltages, due to differences between thermoelectric modules. The "predicted total voltage/power condenser maximum" curve is the theoretical limit for this 12-module system if the evaporator power is not limited. If additional modules were to be added to the system, them the whole condenser curve would be located further up. This results in an increase of power at low HP temperatures, but output power at

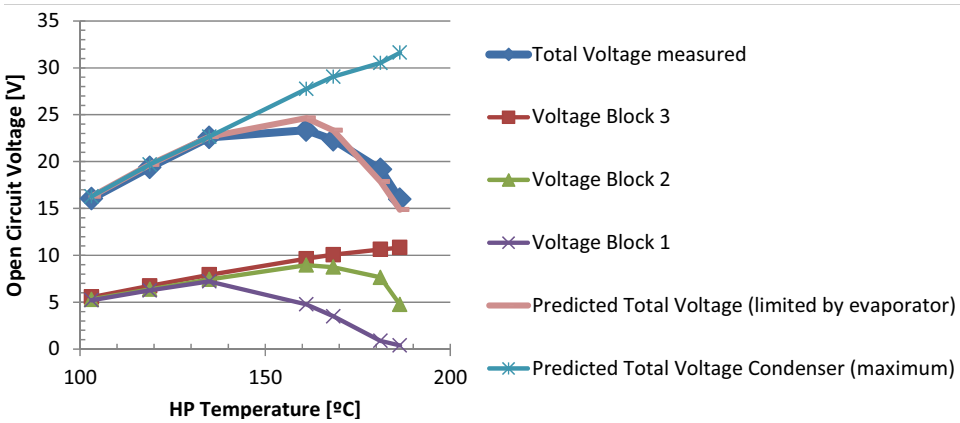

Fig. 14. Theoretical versus experimental steady state open circuit voltage results for the whole HP pressure/temperature range tested.

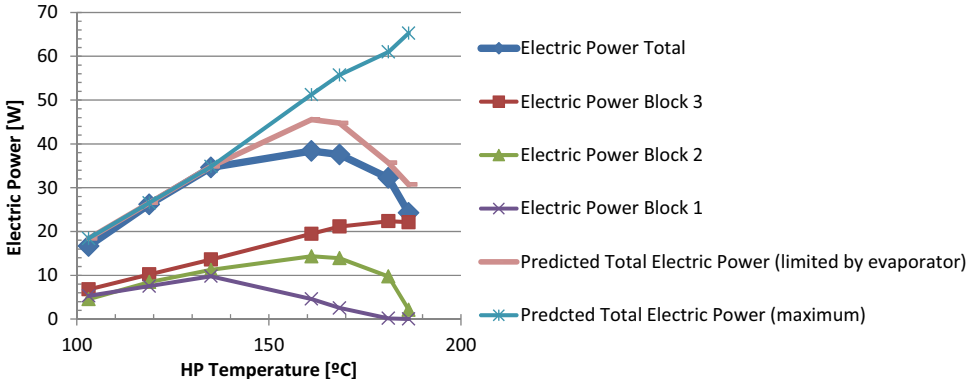

Fig. 15. Theoretical versus experimental steady state maximum power output results for the whole HP pressure/temperature range tested.

high HP temperatures is maintained, due to the evaporator limits.

CONCLUSIONS

A detailed 1D model for assessing the performance of a thermoelectric generator with heat pipe heat exchangers has been proposed and validated with the experimental results of a proof-of-concept model. This model incorporated all major thermal and electric factors affecting thermoelectric module behaviour into a 1D approach, including thermal and electric contact resistances, as well as diffuse and localized (interfacial) heat sources and sinks due to the Peltier/Joule effect.

The use of heat pipes was found to have significant advantages in terms of providing a constant operating temperature, passive protection against overheating and temperature downgrading without the need for heat rejection mechanisms, and of providing a cascading operation without temperature dilution.

At low HP temperatures, the condenser output capacity was found to be the limiting factor for maximizing output. At high HP temperatures, the limiting factor was found to be the evaporator power. So, a high-temperature output may be improved by increasing the evaporator effectiveness or by increasing the exhaust power. The tuning of the operating temperature of the HP was found to be vital to maximizing the output.

Illustrative tests were made with a proof of concept prototype with 12 mass-market bismuth telluride modules attached to a small diesel engine with low exhaust temperature. The thermal performance achieved with this concept opens a good prospect for future scaled-up prototypes working at higher temperatures with higher available exhaust thermal powers, and using novel, higher figure-of-merit modules.

ACKNOWLEDGEMENTS

Project ThinHarvest (FCOMP-01-0124-FEDER-041343/EXPL/EMS-ENE/1023/2013) and post doctoral grant SFRH/BPD/89553/2012, financed by FEDER funds through Programa Operacional Fatores de Competitividade—COMPETE and National funds through PIDDAC and FCT—Fundação para a Ciência e a Tecnologia; Luso-American Foundation/National Science Foundation (FLAD/NSF) 2013 PORTUGAL—U.S. Research Networks Program, Project "Waste Exhaust Energy Recovery of Internal Combustion Engines".

REFERENCES

1. A.E. Atabania, I.A. Badruddina, S. Mekhilefc, and A.S. Silitonga, *Renew. Sust. Energy Rev.* 15, 4586–4610 (2011).
2. B. Ribeiro and J. Martins, SAE Tech. Pap. Ser. No. 2007-01-0261 (SAE Int'l, Warrendale, 2007).
3. J.J.G. Martins, K. Uzuneanu, B. Ribeiro, and O. Jasansky, SAE Tech. Pap. Ser. No. 2004-01-0617, *Modeling of Spark Ignition Engines* (SAE Int'l, Warrendale, 2004).
4. J. Pinto, T. Costa, J. Martins, and F.P. Brito, *New Trends in Mechanism and Machine Science: From Fundamentals to Industrial Applications* (New York: Springer, 2014), pp. 221–232.
5. M. Mori, T. Yamagami, M. Sorazawa, T. Miyabe, S. Takahashi, and T. Haraguchi, SAE Tech. Pap. Ser. No. 2011-01-1335 (SAE Int'l, Warrendale, 2011).
6. J. Martins and F.P. Brito, *Carros Elétricos* (Porto: Publindústria, 2012).
7. J. Martins, *Motores de Combustão Interna*, 4th ed. (Porto: Publindústria, 2013).
8. J. Heywood, *Internal Combustion Engine Fundamentals* (New York: McGraw Hill, 1988).
9. J. Ribau, C. Silva, F.P. Brito, and J. Martins, *Energy Convers. Manag.* 58, 120–133 (2012).
10. L. Bell, *Science* 321, 1457–1461 (2008).
11. D.M. Rowe and G. Min, *IEE Proc. A* 143, 351 (1996).
12. T.C. Hung, T.Y. Shai, and S.K. Wang, *Energy* 22, 661–667 (1997).
13. P. Pichanusakorn and P. Bandaru, *Mater. Sci. Eng. R* 67, 19–63 (2010).
14. C.B. Vining, *Nat. Mater.* 8, 83–85 (2009).
15. G. Min and D.M. Rowe, *IEEE T. Energy Convers.* 22, 528–534 (2007).
16. J.P. Carmo, J. Antunes, M.F. Silva, J.F. Ribeiro, L.M. Goncalves, and J.H. Correia, *Measurement* 44, 2194–2199 (2011).
17. J. Yang and F.R. Stabler, *J. Electron. Mater.* 38, 1245–1251 (2009).
18. J.P. Carmo, L.M. Goncalves, R.F. Wolffenbuttel, and J.H. Correia, *Sensor Actuators A* 161, 204 (2010).
19. M.S. Dresselhaus, G. Chen, M.Y. Tang, and R.G. Yang, et al., *Adv. Mater.* 19, 1043 (2007).

20. F.P. Brito, J. Martins, L.M. Goncalves, N. Antunes, and D. Sousa, *SAE Int. J. Passeng. Cars Mech. Syst.* 6, 2 (2013).
21. F.P. Brito, J. Martins, R. Sousa, and L.M. Gonçalves, *SAE Int. J. Passeng. Cars Electron. Electr. Syst.* 5, 561–571 (2012).
22. D. Reay and P. Kew, *Heat Pipes: Theory, Design and Applications*, 5th ed. (Butterworth-Heinemann Elsevier, New York, 2006), Chapter: Variable conductance heat pipes, pp. 215–218; Chapter: Theoretical background: Heat transfer in the condenser, p. 81; Chapter: Heat transfer and fluid flow theory, pp. 66–67.
23. J. Martins, F.P. Brito, L.M. Goncalves, and J. Antunes, SAE Tech. Pap. Ser. No. 2011-01-0315, (SAE Int'l, Warrendale, 2011).
24. F.P. Brito, J. Martins, L.M. Goncalves, and R. Sousa, *37th IEEE Conference on Industrial Electronics Society* (IECON 2011), November 7–10, Melbourne, Australia (IEEE Xplore, 2011).
25. A. Zukauskas, *Advances Heat Transfer*, Vol. 8, ed. J.P. Hartnett and T.F. Irvine (New York: Academic, 1972).
26. F.P. Incropera and D.P. deWitt, *Fundamentals of Heat and Mass Transfer*, 3rd ed. (Wiley, New York, 1990), Chapter 1—Introduction, p. 4; Chapter 3.5—Conduction with thermal energy generation, pp. 108–110; Chapter 3.6 Heat transfer from extended surfaces, p. 133; Chapter 4.3.3: The conduction shape factor, p. 180; Chapter 8.4.2—The entry region, pp. 494–495.
27. B. Snaith, P.W. O'Callaghan, and S.D. Probert, *Appl. Energy* 16, 175–191 (1984).
28. G.P. Peterson and L.S. Fletcher, *Proceedings of the International Symposium on CoolingTechnology for Electronic Equipment* (Honolulu, 1987), pp. 438–448.
29. M.M. Yovanovich, *Heat Transfer—1986*, Vol. 1, ed. C.L. Tien, V.P. Carey, and J.K. Ferrel (New York: Hemisphere, 1986), .
30. E. Fried, *Thermal Conductivity*, Vol. 2, ed. R.P. Tye (London: Academic, 1969), .
31. D.M. Rowe, *Thermoelectrics Handbook: Macro to Nano*, ed. D.M. Rowe (New York: CRC, 2005), pp. 1-1–1-14.